Online Process Monitoring for Additive Manufacturing Using Eddy Current Testing With Magnetoresistive Sensor Arrays

Henrik Ehlers, Matthias Pelkner, and Roland Thewes, *Senior Member, IEEE*

***Abstract*—The rising popularity of additive manufacturing processes leads to an increased interest in possibilities and methods for related process monitoring. Such methods ensure improved process quality and increase the understanding of the manufacturing process, which in turn is the basis for stable component quality, e.g., required in the aerospace industry or in the medical sector. For laser powder bed fusion, a handful of process monitoring tools already exist, such as optical tomography, thermography, pyrometry, imaging, or laser power monitoring. Although these tools provide helpful information about the process, more information is required for an accurate in-depth understanding. In this article, advanced approaches in eddy current testing (ET) are combined, such as single wire excitation, magnetoresistive (MR) sensor arrays, and heterodyning to build up a system that can be used for online process monitoring of laser powder bed fusion. In addition to detailed information about the developed ET system and underlying signal processing, the first results of magnetoresistance-based online ET during the laser powder fusion process are presented. While producing a step-shaped cuboid, each layer is tested during recoating. Test results show that not only the contours of the topmost layer are detected but also the contours of previous layers covered by powder. At an excitation frequency of 1 MHz, a penetration depth of approx. 400 μm is obtained. To highlight the possibilities of ET for online process monitoring of laser powder bed fusion, results are compared with postexposure images of the integrated layer control system (LCS).**

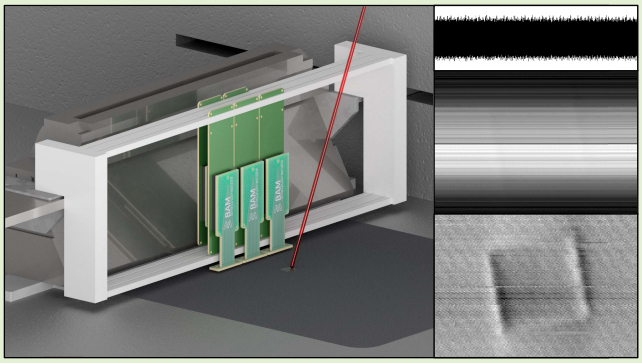

***Index Terms*— Additive manufacturing, eddy current testing (ET), giant magnetoresistance (GMR), Haynes282, heterodyning, laser powder bed fusion (LPBF), nondestructive testing, process monitoring.**

I. Introduction

ADDITIVE manufacturing (AM) recently gained popularity for its possibilities to manufacture prototypes and small batches with complex geometries. For the aerospace industry and for the medical sector, metal parts manufactured using laser powder bed fusion (LPBF) are of high interest [1]. For this reason, research has recently been concerned with the development of new powders and process improvements [1], [2], [3]. Since common problems during manufacturing, like pores, cracks, or delamination, are now well known [4], a number of tools have been developed to help monitor the process, leading to improved part quality, which in turn increases the cost-effectiveness of AM parts [3].

Several process monitoring systems are already commercially available. There are systems for monitoring process parameters, such as oxygen content, temperature, or gas flow, as well as systems that coaxially monitor laser power or add pyrometry, optical tomography, melt pool monitoring, or acoustic emission to the manufacturing equipment [4], [5], [6], [7]. Even though these systems are already of great value for process monitoring and have contributed to the development of stable process parameters [1], there is still a need for additional or improved tools and their integration within the LPBF machine, because cracks, pores, or other buried flaws are not reliably detected by the current technical solutions.

Layer-wise eddy current testing (ET) is a novel approach for process monitoring systems. Although it is possible to test parts embedded in powder with conventional, commercially available ET probes [8], there are some advantages when using magnetoresistive (MR) ET probes. These probes are

Manuscript received 1 August 2022; accepted 6 September 2022. Date of publication 14 September 2022; date of current version 14 October 2022. This work was supported by the Bundesanstalt für Materialforschung und -prüfung within the focus area materials. The associate editor coordinating the review of this article and approving it for publication was Dr. Mert Torunbalci. *(Corresponding author: Henrik Ehlers.)*

Henrik Ehlers and Matthias Pelkner are with the Bundesanstalt für Materialforschung und -prüfung, 12205 Berlin, Germany (e-mail: henrik.ehlers@bam.de).

Roland Thewes is with the Chair of Sensor and Actuator Systems, Faculty of Electrical Engineering and Computer Science (EECS), Technical University of Berlin (TU Berlin), 10623 Berlin, Germany.

Digital Object Identifier 10.1109/JSEN.2022.3205177

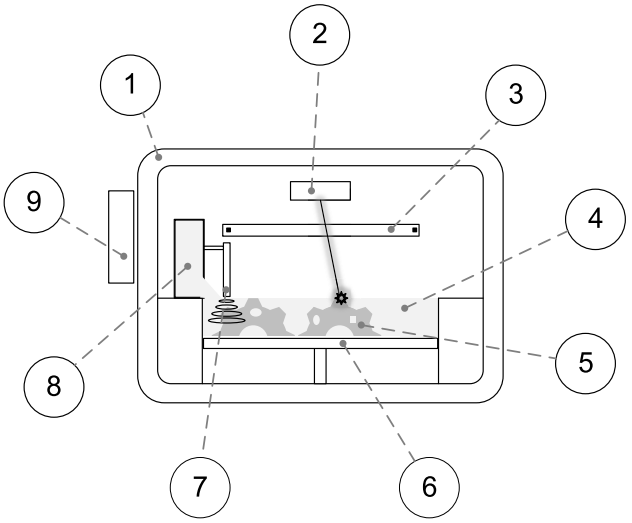

Fig. 1. Simplified sketch of the online ET setup. 1) Build chamber, 2) diode laser, 3) position tracking system, 4) powder, 5) part, 6) build platform, 7) MR probes, 8) recoater, and 9) DAQ and control unit of the system.

of much smaller size than coils, they do not influence each other's signal when densely packed, and can be switched or multiplexed quickly because of their small inductance [9]. Therefore, special hardware and software have been developed for online process monitoring of LPBF-manufactured parts for this application. With recent approaches in ET, such as using MR sensor arrays in combination with single wire excitation, high sensitivity and high spatial resolution can be achieved while maintaining low testing times [10], [11]. Combined with a heterodyne principle, requirements for signal processing hardware and software are lowered enabling compact process monitoring tools [12], [13], [14], [15], [16].

Until now, feasibility has been demonstrated of offline ET of LPBF parts using such systems and their nonexisting influence on the powder [17]. This work provides results of a multilayer online process monitoring additively manufacturing an LPBF component. Beforehand detailed information about the principle of ET process monitoring, the developed system with data acquisition (DAQ), and the processing unit is provided.

II. Online ET Process Monitoring

A. Principle

In order not to interrupt the production process and thus not to increase the production time, ET is carried out during the powder deposition process. This is advantageous in the sense that the movement of the recoater can be used for the ET scan. The basic principle and related components of the ET system are depicted in Fig. 1.

After a new layer of part (5) is exposed by the diode laser (2), a new coat of powder (4) is deposited by the recoater (8), and the ET scan is performed in parallel. To test the whole build platform (6), the complete platform width must be covered by MR probes (7). An ET scan of every layer from the manufacturing process will lead to 3-D defect and geometry information. One particular advantage of ET is, that not only surface defects, but also buried defects can be detected. Therefore, defects can be monitored that heal or emerge later in the production process. Since most LPBF machine manufacturers restrict the access to electrical interfaces of their machines, recoater position or trigger signals cannot be obtained directly but must be acquired by an additional position tracking system (3) that is mounted to the wall of the build chamber (1). Since the build chamber is densely packed and gas flow, temperature, or spatter of the process lead to harsh environmental conditions, the ET system is designed to be modular, so that the DAQ and control unit of the system (9) can be positioned outside.

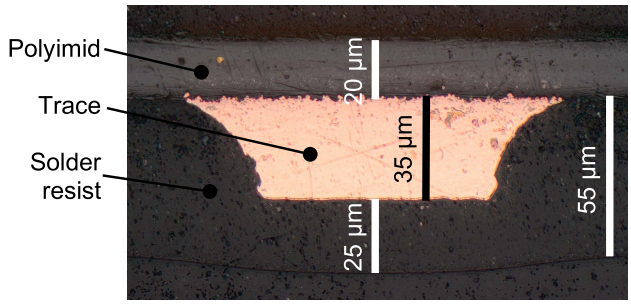

Fig. 2. Cross section of the flexible foil of the rigid-flex PCB showing the trace on polyimide covered by solder resist.

The modular ET system consists of four components: MR probes with single wire excitation, multiplexer, and amplifier printed circuit boards (PCBs) which also enable heterodyning, DAQ shield with an analog-to-digital converter (ADC) and filter, and field-programmable gate array (FPGA) board with SD card storage. In addition, a power supply and a dual-channel function generator are used.

B. MR Probes

MR probes are designed to have a high spatial resolution, provide high sensitivity, and large testing width. To build up the MR probe four giant MR (GMR) arrays are glued at the edge of a PCB with 128 GMR elements in total and a pitch of 125 μm [18], bonded to gold pads, and combined with a single wire excitation.

The MR elements of the array are linear and saturate between -3 and 5 mT. The transfer function of one randomly chosen MR element is as follows:

$$R_{H_Z} = 1.13\frac{\Omega}{\text{mT}} \cdot H_Z + 168.50\ \Omega. \tag{1}$$

Above 10 kHz, the noise of the MR element is approximately 3 nV/.$\sqrt{}$Hz [19].

To precisely induce eddy currents and to make use of the single wire principle, a small conductor must be positioned directly underneath the GMR sensors. A minimal distance from the test surface to GMR elements increases the sensitivity of the MR probe. Hence, a thin wire is advantageous. For improved manufacturability, the single wire excitation is realized on the foil of a rigid-flex PCB. Fig. 2 shows a cross section of the foil. A 20-μm polyimide foil holds the 35-μm-thick copper trace. The width of the trace is 100 μm. There is also a 25-μm solder resist to improve rigidity.

To ensure perfect positioning of the excitation wire, an alignment fixture with six degrees of freedom helps to

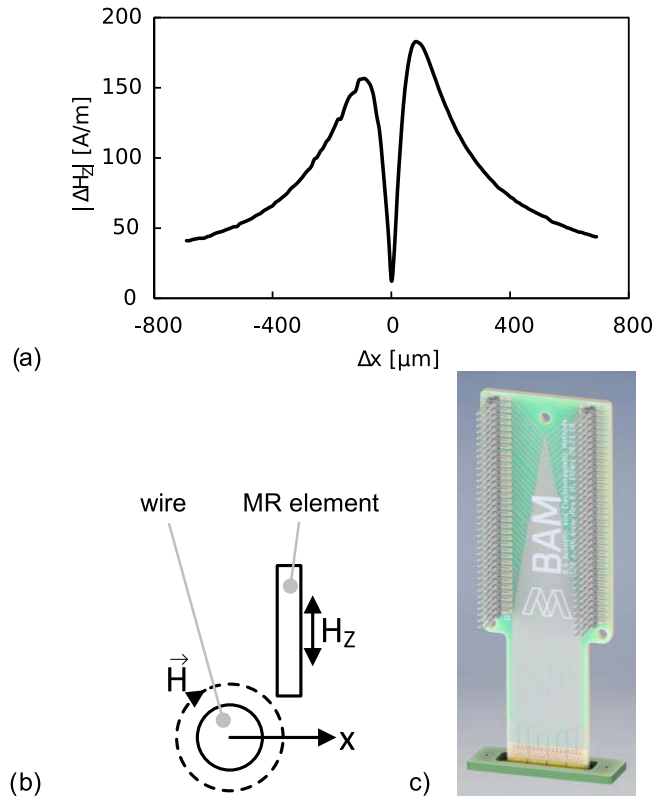

Fig. 3. (a) Absolute magnetic field $|\Delta H_z|$ measured by the MR element as a function of the wire position Δx. (b) Movement of the wire along x-direction and magnetic field H underneath the MR element which is only sensitive to the normal field component H_z. (c) Rendered image of the MR probe.

position the rigid-flex PCB, while the normal field component ΔH_z is measured with the outmost MR elements are measured (c.f. Fig. 3). Optimal alignment is achieved when the measured normal field component ΔH_z is minimized. The MR element is only sensitive to the normal field component ΔH_z and delivers a minimal output signal for a perfectly positioned wire. In this case, the wire is directly under the MR element. The absolute value of the measured field is shown in Fig. 3(a) as a function of the wire position for one MR element. The optimal wire position is at $\Delta x = 0$ μm.

There are two local maxima visible in the curve. Asymmetry in maxima values is visible due to skewed wire movement. The wire is moved as depicted in Fig. 3(b). The wire position is fixed with a two-component adhesive. The complete MR probe is shown as a rendered image in Fig. 3(c). It consists of 128 MR elements with single wire excitation, an MR pitch of 125 μm, and a total testing width of 16 mm. Connection to the MR elements is done via pin headers. The slim design ensures that wider testing widths can be achieved with parallelization in two offset rows.

It has been shown that a similarly constructed probe is able to detect 400-μm EDM blind holes in aluminum and 100-μm wide and 200-μm deep notches in 316L [17].

C. System Design

The underlying system design is depicted in Fig. 4. For improved readability, the modules representations are restricted to their core functionalities and do not show repetitions, which would be necessary to visualize the signal processing of all 128 MR elements. As mentioned in Section II-B, the MR probe is positioned directly over the specimen. One function generator channel delivers the sinusoidal signal for the excitation wire with a frequency f_1.

Multiplexers and amplifiers on a PCB are connected directly to the pin headers of the MR probe. A multiplexer is used per 16 MR elements. Every element is successively switched on for 388 μs and an additional dead time of 1.5 μs is added between switching. This means that at a velocity of 24-mm/s switching of all elements is done over a distance of 150 μm.

For heterodyning, the switched MR elements are part of a Wheatstone bridge configuration with a sinusoidal supply with a frequency f_2. The bridge is tuned with a potentiometer. An instrumentation amplifier with a gain set to 54 dBV is used to amplify the bridge voltage. Fig. 5 shows the module in combination with the MR probe. With eight multiplexers and eight instrumentation amplifiers, all 128 MR elements can be measured. A flat ribbon connector is used to connect the module to the DAQ module. This allows for independent positioning and recoater movement when the module is mounted.

As described in [17], a bandpass filter set to 20 kHz isolates the heterodyne frequency f_3. Switching of MR elements with varying resistance and a high gain instrumentation amplifier lead to a long settling time of the filter. Therefore, a switch connects the input signal of the filter to the ground during switching. To measure the output voltage of every amplifier an eight-channel ADC is used. The ADC can digitize each channel with a sampling rate of 500 kSPS at a resolution of 18 bit, nominally. To process all the data, a Cora Z7 FPGA module based on a Xilinx Zynq-Z000 is used. The parallel processing capability is required to buffer the 72-MB/s data stream of the ADC's parallel interface.

In this first development stage, an SD card is used to store the data. Fig. 6 shows the DAQ module on top of the FPGA board. The switching signal for the multiplexer and switch is generated by the FPGA. Switching times are set up ahead of the measurement and must be considered during signal processing. Start and stop signals for the measurement are generated externally with a position tracking system for the recoater.

Switching times in combination with a constant known recoater speed enable the transfer of the time-based data into location-based data. For every new measurement, a new file with the raw ADC data is stored on the SD card. The data are evaluated afterward on a PC using MATLAB.

D. Software

To demonstrate how the ET data are generated from the raw ADC data on the SD card, the signal processing is illustrated in Fig. 7. The raw data of each file [c.f. Fig. 7(a)] are split into the eight ADC channels [c.f. Fig. 7(b)]. With 16 elements per channel and a known number of samples per element, the data are chopped into frames [c.f. Fig. 7(c)]. Each frame is then handled individually. The overshoot from multiplexing is not fully suppressed by the switch. As a result, a few samples are cut away from each frame [c.f. Fig. 7(d)]. Afterward,

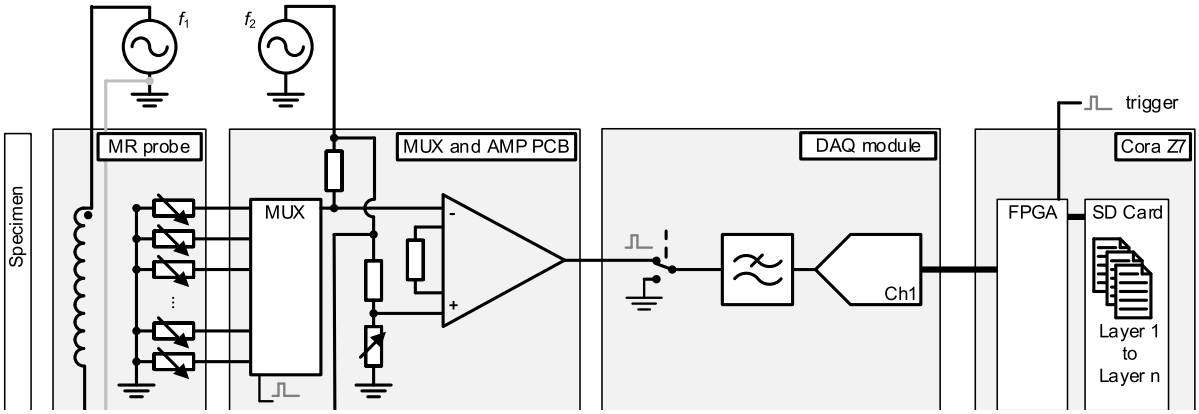

Fig. 4. Simplified system schematic for online ET composed of MR probe with an excitation frequency f_1, multiplexer and amplifier PCB with a Wheatstone bridge for heterodyning operated at a frequency f_2, DAQ module with switch, filter and ADC, and Cora Z7 FPGA board with SD card storage.

Fig. 5. MR probe with 128 MR elements mounted onto the multiplexer and amplifier PCB.

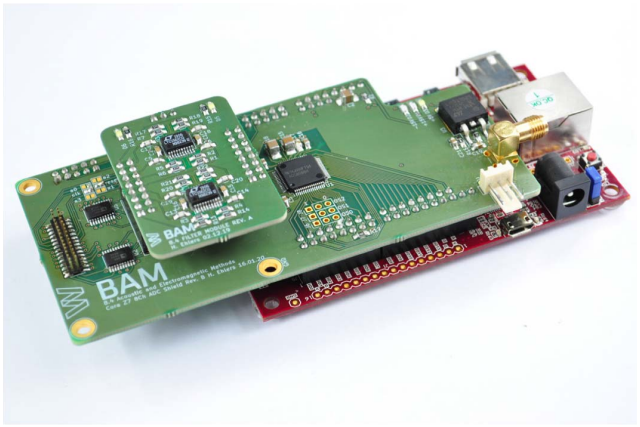

Fig. 6. DAQ module mounted on top of the Cora Z7 FPGA board.

a fast Fourier transform (FFT) is performed [c.f. Fig. 7(e)] and the maximum value is stored [c.f. Fig. 7(f)]. Maximum values of each frame are translated into grayscale images with location information [c.f. Fig. 7(g)]. Offset adjustment is needed because of the varying base resistance and sensitivity of the MR elements [c.f. Fig. 7(h)]. This leads to the ET amplitude image of the measurement.

III. Measurement Setup

Before every manufactured layer of a part can be measured, the ET system needs to be integrated into the LPBF machine. The integrated system is depicted in Fig. 8.

A fixture (5) that is mounted to the recoater (6) holds the MR probe with a multiplexer and amplifier PCB (4). To detect recoater movement and trigger the measurement, a position tracking system (10) is mounted on the side of the build chamber (1).

The DAQ module with FPGA (13), dual-channel frequency generator (12), and power supply (11) is positioned outside the build chamber.

Connections are made via two flat ribbon connectors and a BNC cable. During manufacturing, the build chamber is flooded with argon as shielding gas. Therefore, cables are fed through an airtight cable duct (14). When part (8) is manufactured, the diode laser (3) melts the powder (7) that is deposited over the build platform (9). The integrated layer control system (LCS) (2) takes an optical image of the exposed layer. Afterward, the build platform is lowered and a new layer of powder is deposited. The ET is performed during this recoating process. Fig. 9(a) and (b) shows the images from inside and outside the build chamber ahead of the measurement.

A. Adjustment of the MR Probe

For a sensitive ET, a minimal lift-off between test specimen and MR probe is required. This adjustment is done by shifting the fixture up or down. The set lift-off for the measurement results in marks of the MR probe in the powder bed. However, this is not optimal for the manufacturing process and must be avoided for future testing. This effect is visible in the image of the LCS (see Fig. 10).

B. Parameters and Test Specimen

A 3.4-mm step-shaped cuboid with a 10 mm × 10 mm base and two 1-mm diameter holes is chosen as a test specimen [see Fig. 11(a) and (b)]. It is manufactured from Haynes282 powder with an SLM280 HL machine. The conductivity σ of Haynes282 is 0.793 MS/m and the permeability μ_r

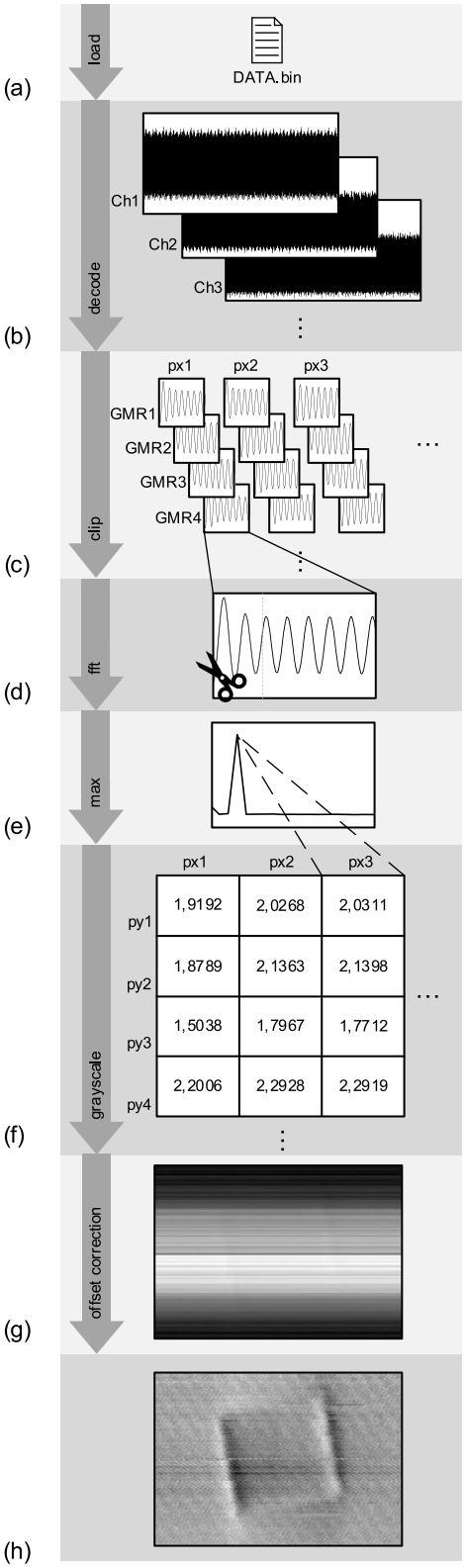

Fig. 7. Applied signal processing to generate ET amplitude imagesfrom raw ADC data acquired during online ET with (a) loading the raw data, (b) decoding data into individual pixels, (c) clipping for improved signal integrity, (d) performing an FFT, (e) taking the maximum value, (f) converting values into a grayscale image, (g) applying an offset correction to recieve, and (h) ET amplitude image.

is ∼1. These parameters determine the penetration depth and, therefore, the ET signals. The manufacturing parameters are listed in Table I. An additional 4-mm solid support structure

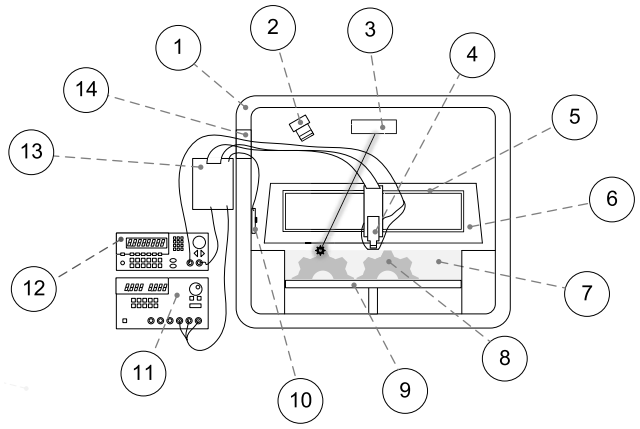

Fig. 8. Simplified sketch of the measurement setup. 1) Build chamber, 2) layer control system, 3) diode laser, 4) MR probe with multiplexer and amplifier PCB, 5) fixture, 6) recoater, 7) powder, 8) part, 9) build platform, 10) position tracking system, 11) power supply, 12) dual-channel frequency generator, 13) DAQ module with FPGA, and 14) cable duct.

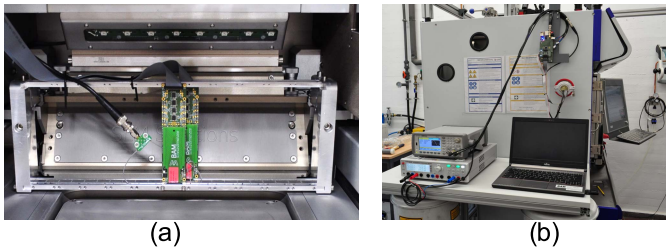

Fig. 9. (a) MR probes on fixture mounted to recoater inside build chamber of LPBF machine. (b) DAQ module and FPGA board with power supply and frequency generator outside of LPBF machine.

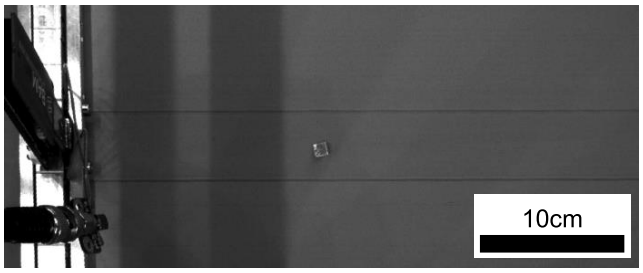

Fig. 10. Postexposure image taken by the LCS with MR probe and fixture on the left, part in the center and marks in the powder as horizontal lines.

TABLE I
MANUFACTURING PARAMETERS FOR HAYNES282-SLM-STEP SPECIMEN

Parameter	Value
layer height	40 µm
laser power	285 W
scan velocity	850 mm/s
hatch distance	100 µm
exposure strategy	stripes (67° rotation every layer), 2 contour scans
powder	Haynes282 gas-atomized

is manufactured prior to the specimen leading to a height of 7.4 mm and a total of 185 manufactured layers. The specimen is rotated 12° around the z-axis. No additional heating for the build platform and chamber is used.

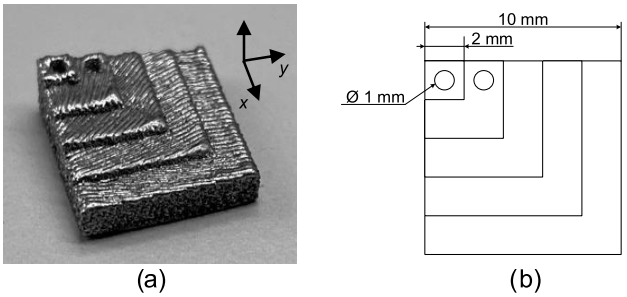

Fig. 11. (a) Image of the specimen after manufacturing and removal of build platform. (b) 2-D drawing of top side of test specimen showing dimensions in *x*- and *y*-directions.

To be able to test the specimen with the system described under Section II-C at a resolution of 135 μm in recoating direction, recoating speed is reduced to 1/10th of the normal recoating speed, resulting in ∼24-mm/s recoater velocity (true recoater velocity cannot be obtained from the machine).

ET is done at frequencies $f_1 = 1$ MHz and $f_2 = 980$ kHz, resulting in a heterodyne frequency $f_3 = 20$ kHz. The excitation frequency is limited by the hardware. A higher excitation frequency is advantageous to better isolate defects near the surface. The estimated penetration depth is 565 μm. However, real penetration depth is smaller because the calculation is based on analyzing eddy currents excited in a half-space conductor. The current through the MR elements is set to $I_{\mathrm{MR}} = 5\ \mathrm{mA_{pp}}$ and the excitation current is set to $I_{\mathrm{Wire}} = 400\ \mathrm{mA_{pp}}$.

IV. Results

During manufacturing of the specimen, all 185 layers are tested by the ET system. The ET data are processed afterward using the methods described in Section II-D. Processed data of significant layers are shown in the following. A strip of 16-mm width and 86-mm length is tested, but the results shown here display a 16 mm × 23 mm section at a resolution of 128 × 170 pixels with each pixel representing 125 μm × 135 μm. In addition, after each exposure, the LCS takes an optical image. The image is cropped to the corresponding 16 mm × 23 mm area to be comparable to the ET results. The cropped image has a resolution of 86 × 121 pixels with each pixel representing an area of 190 μm × 190 μm and is, therefore, lower resolution compared with the ET system. ET results of the first layer with a height of 40 μm above the build platform are given in Fig. 12. The edges of the specimen in parallel to the excitation wire can be detected. Edges perpendicular to the excitation wire are not as pronounced, because the deflection of the eddy currents in this scenario is lower (note that using the expressions "parallel" and "perpendicular" is not completely correct due to the 12° rotation). Reduced deflection can be circumvented by alternative excitation geometries.

Since an absolute single wire MR probe is used, the ET signals of the detectable edges have a differential signature which is typical [15]. The corresponding LCS image is shown in Fig. 13. The outside geometry is visible. A diagonal line from one edge of the specimen to the other is visible. This is due to the exposure strategy. The diagonal line also becomes

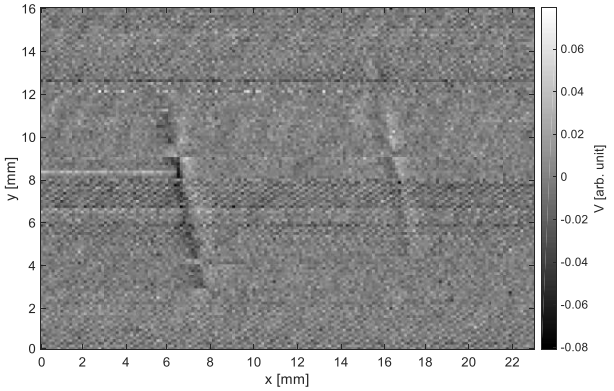

Fig. 12. Online ET amplitude image of layer 1.

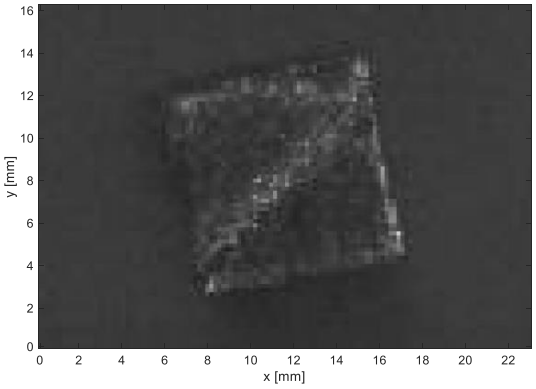

Fig. 13. Postexposure LCS image of layer 1.

apparent in the ET results which is promising. ET results of layer 164 with a height of 6.56 mm above the build platform are shown in Fig. 14. The SNR of the left edge of the specimen to the surrounding area is 5.1 dB. The results also show the differential characteristics of the MR probe. In the ET results not only the edges of the topmost layer are visible but also the edges of the underlying layers of the step-shaped geometry are detectable. Due to the edge effect of the MR probe, the two 1-mm diameter holes near the edges are not detected. At a frequency $f_1 = 1$ MHz, layers in a depth of up to 400 μm can be tested. The corresponding LCS image is shown in Fig. 15. The outside geometry of the topmost layer is visible. Underling layers are not visible because they are covered by powder and hence not detectable for an optical system. The two 1-mm diameter holes are not visible because of the low resolution of the LCS.

In Fig. 16, the ET results of layer 173 are depicted. In this layer, the two 1-mm holes are 1.12-mm deep. They are slightly visible in the ET image. However, a quantitative statement cannot be made since they are superimposed by the edge effect of the probe. Edge information of the underlying layers is reduced because the distance to the surfaces of the underlying layers is increased due to the advancing manufacturing process. The corresponding LCS image is shown in Fig. 17. The geometry of the top layer is visible. Due to the limited resolution, the 1-mm holes are not clearly visible.

Compared with the LCS image simultaneous ET of multiple layers combined with a higher resolution, the ET system is

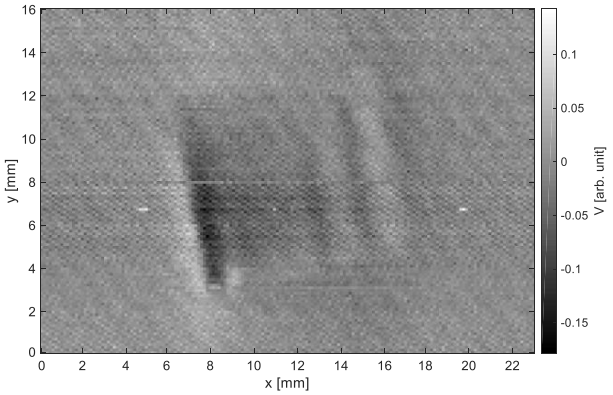

Fig. 14. Online ET amplitude image of layer 164.

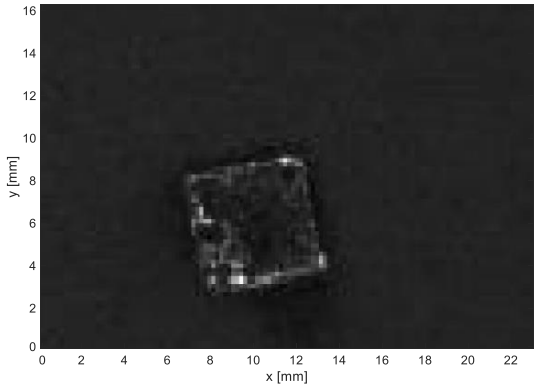

Fig. 15. Postexposure LCS image of layer 164.

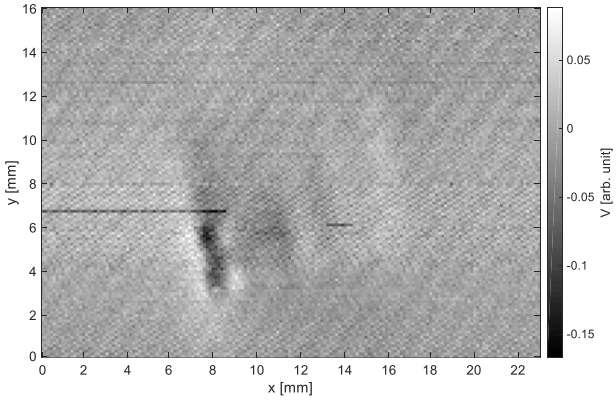

Fig. 16. Online ET amplitude image of layer 173.

advantageous, which is promising given the fact that this has been the first integration of an MR-based ET system for online monitoring of LPBF parts.

V. Discussion

The experiment demonstrates that online ET using MR arrays as sensing elements is a suitable process monitoring tool for AM parts. With the developed system, layer-wise ET can be implemented into LPBF machines. For a first integration and measurement, the results are promising. The ET data in Fig. 12 and in Fig. 14 reveal that not only edges and geometry of the topmost layer can be detected but also the edges of underlying layers. Due to the edge effect of

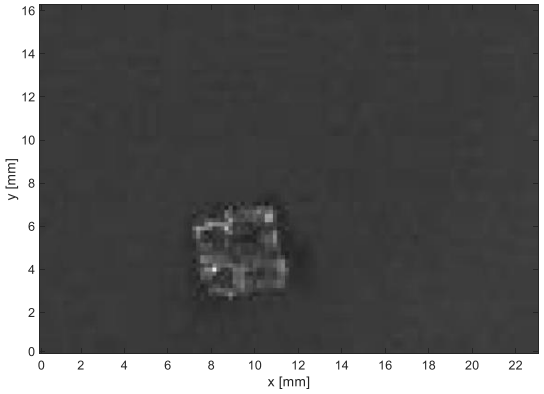

Fig. 17. Postexposure LCS image of layer 173.

the MR probe, holes near edges can be separated from the edges when they are 1.12-mm deep (c.f. Figs. 15 and 16). There are no pores, cracks, or delamination effects visible in any of the ET results. However, since defects such as pores are very likely to occur in the test specimen, a comparative measurement with computed tomography can be used to determine the magnitude of the defects that can be detected. The consequences of the harsh environmental conditions inside the build chamber are not visible in the ET results. The temperature inside the build chamber increases during the manufacturing process from 36.7 °C to 40 °C. Although the surface temperature of the specimen is much higher, the measurement system is insensitive to temperature-dependent effects. Spattering particles in the process are blown away by the gas flow and do not harm the electronics. A modular system design is advantageous for evaluating different MR arrays or alternative excitation geometries. Proper adjustment of the MR probe is a crucial parameter that has to be carefully optimized. This is reflected in the marks in the powder bed (cf. Fig. 10). An optimized fixture that allows micro adjustments after integration can minimize this effect. When multiple MR probes are used adjustment for leveling the MR probes can be necessary in advance.

VI. Conclusion

It has been shown that MR-based online ET for LPBF is feasible with the developed system. The modular system consisting of MR probes, amplifiers, and DAQ is compact and can be integrated into the LPBF machine without significantly affecting the production process. The sensitive custom MR array probe with single wire excitation can detect the specimen's geometry of the first layer. In the further manufacturing process, not only the most recent layer is tested, but also the ten underlying layers. The temperatures during the process do not have a discernible influence on the ET.

Using the proposed simple system design, researchers can recreate online ET for LPBF parts to optimize, improve, and speed up the development of this promising process monitoring tool. Offline signal processing proves to be an uncomplicated and economical solution. For the online ET method to reach its full potential, the ET data must be aligned and compared with the target geometry data of the parts.

Outlook

Moving from discrete to integrated electronics with an adapted system design can lead to lower noise for improved detectability of defects and higher testing speeds for seamless integration. The miniaturization enables future integration into different machines and the extension to full build platform width. Implementing the offline data processing into the FPGA and connecting it to the machine via a suitable interface allows the user to visualize ET results during manufacturing and which is a further step toward process control of LPBF.

Acknowledgment

The authors would like to thank R. Pohl, A. Knöppchen, S. Gohlisch, G. Mohr, B. Merz, T. Räpke, S. Altenburg, T. Renner, and N. Krackow at the Federal Institute for Materials Testing and Research (BAM), Berlin, Germany, and S. Keil at the Technical University of Berlin (TU Berlin), Berlin, for supporting this work.

References

[1] A. Khorasani, I. Gibson, J. K. Veetil, and A. H. Ghasemi, "A review of technological improvements in laser-based powder bed fusion of metal printers," *Int. J. Adv. Manuf. Technol.*, vol. 108, no. 1, pp. 191–209, 2020.

[2] S. Vock, B. Klöden, A. Kirchner, T. Weißgärber, and B. Kieback, "Powders for powder bed fusion: A review," *Prog. Additive Manuf.*, vol. 4, no. 4, pp. 383–397, 2019.

[3] M. Mani, B. Lane, A. Donmez, S. Feng, S. Moylan, and R. Fesperman, "Measurement science needs for real-time control of additive manufacturing powder bed fusion processes," U.S. Dept. Commerce, Nat. Inst. Standards Technol., Tech. Rep. NISTIR8036, 2015.

[4] M. Grasso and B. M. Colosimo, "Process defects and *in situ* monitoring methods in metal powder bed fusion: A review," *Meas. Sci. Technol.*, vol. 28, no. 4, pp. 1–40, 2017.

[5] G. Mohr *et al.*, "*In-situ* defect detection in laser powder bed fusion by using thermography and optical tomography—Comparison to computed tomography," *Metals*, vol. 10, no. 1, p. 103, 2020.

[6] Y. Chivel, M. France, and I. Smurov, "SLS-process monitoring and adaptive control," Tech. Rep., Aug. 2015.

[7] J.-P. Kruth, J. Duflou, P. Mercelis, J. Van Vaerenbergh, T. Craeghs, and J. De Keuster, "On-line monitoring and process control in selective laser melting and laser cutting," in *Proc. 5th Lane Conf. Laser Assist. Net Shape Eng.*, 2007, vol. 1, no. 1, pp. 23–37.

[8] E. I. Todorov, "Non-destructive evaluation of additive manufacturing components using an eddy current array system and method," U.S. Patent 20160349215 A1, Dec. 1, 2016.

[9] T. Dogaru and S. T. Smith, "Edge crack detection using a giant magnetoresistance based eddy current sensor," *Nondestruct. Test. Eval.*, vol. 16, no. 1, pp. 31–53, Jan. 2000.

[10] R. Hamia, C. Cordier, S. Saez, and C. Dolabdjian, "Eddy-current nondestructive testing using an improved GMR magnetometer and a single wire as inducer: A FEM performance analysis," *IEEE Trans. Magn.*, vol. 46, no. 10, pp. 3731–3737, Oct. 2010.

[11] J. Paul, C. Gebhardt, S. Raukopf, M. Kreutzbruck, A. Neubauer, and M. Pelkner, "Sensor arrangement for eddy-current testing of electrically conductive objects to be measured," WO Patent 2015177341 A1, Nov. 26, 2015.

[12] C. Fermon, M. Pannetier, N. Biziere, F. Vacher, and T. Sollier, "Method and device for non destructive evaluation of defects in a metallic object," EP Patent 1991862 B1, Jul. 10, 2013.

[13] D. M. Caetano, M. Piedade, and J. Graça, "A CMOS ASIC for precise reading of a magnetoresistive sensor array for NDT," *11th Eur. Conf. Non-Destructive Test. (ECNDT)*, 2014, pp. 1–10.

[14] L. S. Rosado, F. A. Cardoso, S. Cardoso, P. M. Ramos, P. P. Freitas, and M. Piedade, "Eddy currents testing probe with magneto-resistive sensors and differential measurement," *Sens. Actuators A, Phys.*, vol. 212, pp. 58–67, Jun. 2014.

[15] M. Pelkner *et al.*, "Eddy current testing with high-spatial resolution probes using MR arrays as receiver," in *Proc. 7th Int. Symp. NDT Aerosp.*, 2015, pp. 1–8.

[16] D. M. Caetano *et al.*, "High-resolution nondestructive test probes based on magnetoresistive sensors," *IEEE Trans. Ind. Electron.*, vol. 66, no. 9, pp. 7326–7337, Sep. 2018.

[17] H. Ehlers, M. Pelkner, and R. Thewes, "Heterodyne eddy current testing using magnetoresistive sensors for additive manufacturing purposes," *IEEE Sensors J.*, vol. 20, no. 11, pp. 5793–5800, Jun. 2020.

[18] *Integrated Magnetic Imagery Based on Spintronics Components (IMAGIC), 7th Framework Program, Project Number 288381.*

[19] *IMAGIC 2nd Periodic Report*, 2013.

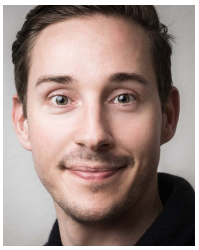

Henrik Ehlers received the master's degree in mechatronics from the Beuth University of Applied Sciences Berlin (BHT), Berlin, Germany, in 2014. He is currently pursuing the Ph.D. degree with the Technical University of Berlin (TU Berlin), Berlin.

From 2014 to 2018, he worked as a Hardware Design Engineer in the fields of high-power laser diode drivers and SoC-based industrial vision at Scansonic MI GmbH, Berlin. Since 2015, he has held many lectures regarding basics of mechatronics, electrical components, and microcomputers at BHT. Since 2018, he has been with the Federal Institute for Materials Testing and Research (BAM), Berlin. He has specialized in eddy current testing for additive manufacturing, which is also his Ph.D. topic.

Matthias Pelkner received the Diploma and Ph.D. degrees in physics from the Technical University of Munich, Munich, Germany, in 2008 and 2014, respectively. He specialized in semiconductor physics and magnetism.

Afterward, he has started to work with the Federal Institute for Materials Testing and Research (BAM), Berlin, Germany, in 2009. Since 2014, he has been part of the Division 8.4 Acoustic and Electromagnetic Methods, Eddy Current Testing Group, BAM. He is responsible for electromagnetic testing and magnetic material characterization. His research work interests include sensor development, simulation, and data analysis for electromagnetic nondestructive evaluation.

Roland Thewes (Senior Member, IEEE) received the Dipl.-Ing. and Dr.-Ing. degrees in electrical engineering from the Technical University of Dortmund, Dortmund, Germany, in 1990 and 1995, respectively.

In 1994, he joined the Research Laboratories, Siemens AG, Munich, Germany, where he was active in the design of nonvolatile memories and in the field of reliability and yield of analog CMOS circuits. From 1997 to 1999, he managed projects in the fields of design for manufacturability, reliability, analog device performance, and analog CMOS circuit design. From 2000 to 2005, he was responsible for the Laboratory on Mixed-Signal Circuits of Corporate Research of Infineon Technologies, Neubiberg, Germany, focusing on CMOS-based biosensors, low-voltage analog CMOS circuit design, and device–circuit interaction. From 2006 to March 2009, he was heading the department focusing on DRAM core circuitry in the Product Development Division, Qimonda, Germany. Since April 2009, he has been a Professor with the Technical University of Berlin (TU Berlin), Berlin, Germany, focusing on CMOS-based sensor systems. He has authored or coauthored more than 160 peer-reviewed technical publications and authored or coauthored a similar number of granted patents and patent applications.

Dr. Thewes served as an Elected Member of the IEEE SSCS AdCom. He is a member of the German Association of Electrical Engineers and the German Academy of Science and Engineering. He was a recipient of the German President's Future Award in 2004 and the ISSCC 2002 Jack Raper Award in 2003, and a recipient or a co-recipient of eight further paper and conference awards. He has been serving on the Technical Program Committees for various conferences, among these IEEE IEDM, IEEE ISSCC, IEEE ESSCIRC, and IEEE BioCAS.